The Large Hadron Collider (LHC) is expected to begin operation around 2007 with proton-proton collisions at 14 TeV center-of-mass energy. A luminosity of 300 inverse femtobarns is expected to be achieved, making the prospects for discovering new physics at the LHC excellent. Numerous classes of models which provide interesting dark matter candidates will be tested at this very important experiment, searching at scales of up to several TeV. In addition to the Higgs boson(s), the LHC will be sensitive to most supersymmetry scenarios, models with TeV-scale universal extra dimensional, little Higgs models, etc.

For a few examples of studies which discuss the sensitivity of the LHC to new physics, see Refs.[42, 148, 168, 23, 24, 46, 284, 398, 102]. In Fig. 16, an example of such a study is shown [46]. It is interesting to note that in the region of the MSSM which is the most difficult to probe at the LHC, direct dark matter detection rates are very high [45].

- *Beyond the LHC*

  After the LHC, other collider experiments are likely to follow. Although no specific post-LHC program is certain at this time, a 500-1000 GeV linear collider is a possibility, perhaps followed by a Very Large Hadron Collider (VLHC). These or other post-LHC colliders will, of course, have great value to particle dark matter studies [464, 63].

# 4 Experiments

## 4.1 Direct Detection Experiments

Direct detection experiments appear today as one of the most promising techniques to detect particle dark matter. The idea is very simple: if the galaxy is filled with WIMPs, then many of them should pass through the Earth, making it possible to look for the interaction of such particles with matter, e.g. by recording the recoil energy of nuclei, as WIMPs scatter off them [191, 254].

The key ingredients for the calculation of the signal in direct detection experiments are the density and the velocity distribution of WIMPs in the solar neighborhood and the WIMP-nucleon scattering cross section. With this information, it is then possible to evaluate the rate of events expected in an experiment (*i.e.* WIMP–nucleon scattering events) per unit time, per unit detector material mass.

The rate is approximately given by

$$R \approx \sum_i N_i n_\chi < \sigma_{i\chi} >, \tag{88}$$

where the index, $i$, runs over nuclei species present in the detector

$$N_i = \frac{\text{Detector mass}}{\text{Atomic mass of species } i}$$

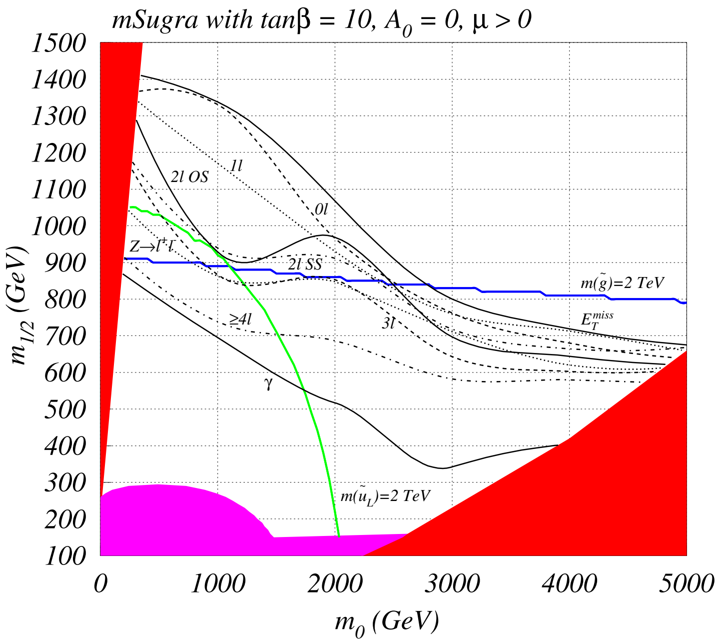


Figure 16: An example of the reach of the Large Hadron Collider (LHC) to new TeV-scale physics [46]. As a function of $m_0$ and $m_{1/2}$ in the mSUGRA (or constrained MSSM) scenario, with $\tan\beta = 10$, $A_0 = 0$ and positive $\mu$, the reach is shown for a variety of channels: zero leptons ($0l$), one lepton ($1l$), leptons with opposite charge ($OS$), leptons with the same charge ($SS$), three leptons ($3l$), four or more leptons ($\geq 4l$), any number of leptons plus a photon ($\gamma$), at least two opposite sign leptons with the invariant mass within an optimized interval around the $Z$ mass ($Z \to l^+l^-$) and an "inclusive" missing transverse energy channel. Also shown are the 2 TeV up squark and 2 TeV gluino mass contours. The red regions are excluded by theoretical constraints, while the magenta region is excluded experimentally. 100fb$^{-1}$ of integrated luminosity is assumed.

is the number of target nuclei in the detector,

$$n_\chi \equiv \frac{\text{WIMP energy density}}{\text{WIMP mass}}$$

is the local WIMP density and $< \sigma_{i\chi} >$ is the cross section for the scattering of WIMPs off nuclei of species $i$, averaged over the relative WIMP velocity with respect to the detector. For a more through discussion see, *e.g.* , Ref. [305].

### 4.1.1 Scattering classifications

The type of scattering processes considered can be classified by two important characteristics: elastic or inelastic scattering and spin-dependent or spin-independent scattering.

- Elastic and Inelastic Scattering

  The elastic scattering of a WIMP off of a nucleus in a detector is simply the interaction of the WIMP with a nucleus as a whole, causing it to recoil, ideally often enough to measure the recoil energy spectrum in the target. With a Boltzman velocity distribution of WIMPs, centered at 270 km/s, the spectrum of recoils is exponential with typical energies of $< E > \sim 50\,\text{keV}$. Current experiments can detect recoils of considerably lower energy, as low as 1-10 keV.

  Inelastic scattering, on the other hand, is not observed by the recoil of a target nuclei. Instead, the WIMP interacts with orbital electrons in the target either exciting them, or ionizing the target. Alternatively, the WIMP could interact with the target nuclei leaving it in an excited nuclear state. This process leaves the signature of a recoil followed by the emission of a photon a nanosecond, or so, later [201]. Such signatures have to compete with backgrounds of natural radioactivity, however.

- Spin-Dependent and Spin-Independent Scattering

  WIMP scattering off of nuclei is commonly discussed in the context of two classes of couplings. First, axial-vector (spin dependent) interactions result from couplings to the spin content of a nucleon. The cross sections for spin-dependent scattering are proportional to J(J+1) rather than the number of nucleons, so little is gained by using heavier target nuclei. For scalar (spin-independent) scattering, however, the cross section increases dramatically with the mass of the target nuclei, and typically dominates over spin-dependent scattering in current experiments which use heavy atoms as targets.

  It should be pointed out that a WIMP which is not a Majorana particle could also scatter by vector interactions. Heavy Dirac neutrinos or MSSM sneutrinos are examples of particles which would scatter in this way. Neutralinos and Kaluza-Klein dark matter do not have such couplings, however.

For more on scalar, axial-vector and vector WIMP-nucleon scattering, see Appendix C.

### 4.1.2 Experimental Efforts

More than 20 direct dark matter detection experiments are either now operating or are currently in development. In these many experiments, numerous techniques have been developed to measure the nuclear recoil produced by dark matter scattering. Some of these methods include the observation of scintillation (used by DAMA, ZEPLIN-I, NAIAD, LIBRA), photons (used by CREST and CUORICINO) and ionization (used by HDMS, GENIUS, IGEX, MAJORANA and DRIFT). Some experiments use multiple techniques, such as CDMS and Edelweiss which use both ionization and photon techniques, CRESST-II and ROSEBUD which use both scintillation and photon techniques and XENON, ZEPLIN-II, ZEPLIN-III and ZEPLIN-MAX, which use both scintillation and ionization techniques.

The use of such a large array of techniques and technologies is important not only to accelerate the progress of the field, but also to vary the systematic errors from experiment to experiment, allowing for a critical assessment of a positive signal.

Some experiments are also attempting to separate WIMP signatures from background by looking for an annual modulation in their rate. Such an effect would arise due to the Earth's annual motion around the Sun, resulting in a relative velocity relative to the galaxy's frame of reference. Under this effect, the Earth's velocity is given by

$$v_{\rm E} = 220\,{\rm km/s}\left(1.05 + 0.07\cos(2\pi({\rm t}-{\rm t_m}))\right), \tag{89}$$

where $t_m$ is roughly the beginning of June and the times are in units of years. The result of this effect is a $\cong$ 7% variation in the WIMP flux and direct detection rate over the course of the year. Since this variation is quite small, many events are needed to identify such a signature. For more on this technique and the status of direct detection techniques, see section 5.

## 4.2 Gamma-Ray Experiments

In addition to detecting WIMPs directly, efforts are underway to attempt to observe the products of WIMP annihilations in the galactic halo, the center of the Sun or other regions. These annihilation products include neutrinos, positrons, anti-protons and gamma-rays.

To observe cosmic gamma-rays directly, observations must be made from space. This is because in the energy range we are most interested (GeV to TeV), photons interact with matter via $e^+e^-$ pair production, which leads to an interaction length of approximately 38 g cm$^{-2}$, which is much shorter than the thickness of the Earth's atmosphere (1030 g cm$^{-2}$). Thus, at the energies we are considering, gamma-rays cannot reach ground based telescopes. Efforts have been developed, nevertheless, to observe gamma-rays indirectly with ground based experiments. In this section, we discuss the status of both ground and space-based gamma-ray telescopes.

### 4.2.1 Ground-based telescopes

When photons interact in the atmosphere, they produce an electromagnetic cascade and thus a shower of secondary particles, allowing ground-based telescopes to *indirectly* observe gamma-rays through the detection of secondary particles and the Cerenkov light originating from their passage through the Earth's atmosphere.

It was P. Blackett (winner of the Nobel prize in 1948) who first realized the possibility of detecting Cerenkov light from cosmic air showers. This realization was experimentally confirmed by W. Galbraith and J. Jelley (1953). Cosmic gamma-rays can be difficult to observe in this way, however, as most of the observed Cerenkov light is due to cosmic-ray induced showers with isotropic arrival directions. For detecting gamma-ray showers, an excess above the isotropic background of cosmic rays must be seen in the direction of a source. To accomplish this, the rejection of cosmic ray showers is of crucial importance.

To distinguish between cosmic ray and gamma-ray induced air showers, the observed Cerenkov light is compared with numerical simulations of atmospheric showers (see Fig. 17). Apart from the difficulties in the treatment of interactions at very high energies, numerical simulations are complicated by uncertainties associated with the density profile of the atmosphere and the Earth's magnetic field. Nevertheless, reliable codes for simulating atmospheric showers exist on the market, for example CORSIKA and AIRES (see *e.g.* Knapp *et al.* [321]).

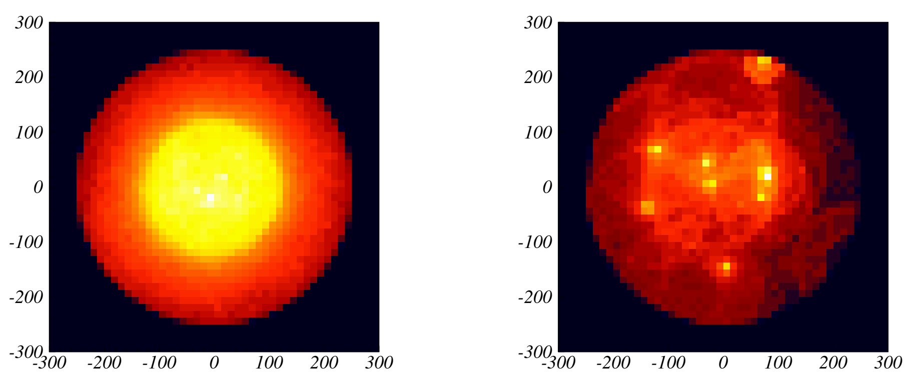


Figure 17: Simulations of Cerenkov light from electromagnetic cascades initiated by a 1 TeV photon (left) and a 1 TeV proton (right). The figures show the distribution of light to the ground in a $600 \times 600$ m$^2$ area. Figures kindly provided by I. Perez.

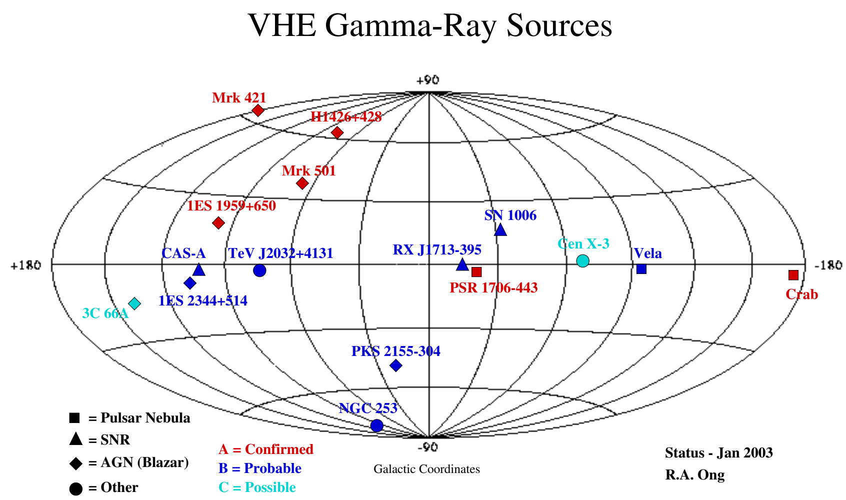


Figure 18: Sky Map for sources of very high-energy (TeV) gamma-rays, as of January 2003 (Ref. [386]).

The methods of collecting Cerenkov light are quite varied, ranging from telescopes (and array of telescopes) to converted solar arrays. We show in table 6 a list of existing ground based experiments for the detection of gamma-rays. These include imaging and non–imaging Air Cerenkov telescopes, reconverted solar arrays as well as experiments which detect secondary particles produced in showers.

The first observation of Cerenkov light due to gamma-ray emission from an astrophysical source was the detection of the Crab Nebula (which today is regarded as the "standard candle" at these energies) with the Whipple Observatory 10m reflector [462]. Currently, only six TeV gamma-ray sources have been *confirmed*, above 10 GeV, having been detected by multiple experiments at a high significance level (red symbols in Fig. 18). Eight sources are *probable*, *i.e.* detected at high significance by at least one group (blue symbols), and two are "possible" (light blue symbols, see Ref. [386] for more details).

Although only a few TeV gamma-ray sources have been confirmed, many more could be detected in next generation experiments. Among these experiments:

- MAGIC is a 17m imaging air Cerenkov telescope recently completed on the island of La Palma [483]. It has already started taking data.

| *Imaging* | | | | |
|---|---|---|---|---|
| Group | Location | Telescope(s) Num.×Apert. | Threshold (TeV) | Ref. |
| Whipple | Arizona, USA | 10 m | 0.4 | [134] |
| Crimea | Ukraine | 6×2.4 m | 1 | [457] |
| SHALON | Tien Shen, Ru | 4 m | 1.0 | [380] |
| CANG-II | Woomera, Au | 10 m | 0.5 | [276] |
| HEGRA | La Palma, Es | 5×5 m | 0.5 | [164] |
| CAT | Pyrenées, Fr | 4.5 m | 0.25 | [255] |
| TACTIC | Mt. Abu | 10 m | 0.3 | [92] |
| Durham | Narrabri | 3×7 m | 0.25 | [137] |
| 7TA | Utah, USA | 7×2 m | 0.5 | [473] |

| *Non-Imaging* | | | | |
|---|---|---|---|---|
| Group | Location | Type | Telescopes | Ref. |
| Potchefstroom | South Africa | Lateral Array | 4 | [172] |
| Pachmarhi | India | Lateral Array | 25 | [93] |
| Beijing | China | Double | 2 | [474] |

| *Solar Arrays* | | | | |
|---|---|---|---|---|
| Group | Location | Heliostats Now (future) | Threshold GeV | Ref. |
| STACEE | Albuq., USA | 32 (48) | 180 | [387] |
| CELESTE | Themis, Fr | 40 (54) | 50±10 | [173] |
| Solar-2 | Barstow, USA | 32 (64) | 20 | [481] |

| *Non - air Cerenkov* | | | | |
|---|---|---|---|---|
| Group | Location | Telescope | Threshold TeV | Ref. |
| Milagro | Fenton Hill, US | Water Cher. | 0.5-1.0 | [475] |
| Tibet HD | Tibet | Scintillators | 3 | [28] |

Table 6: Atmospheric Cerenkov Imaging Observatories *circa* September 2003.

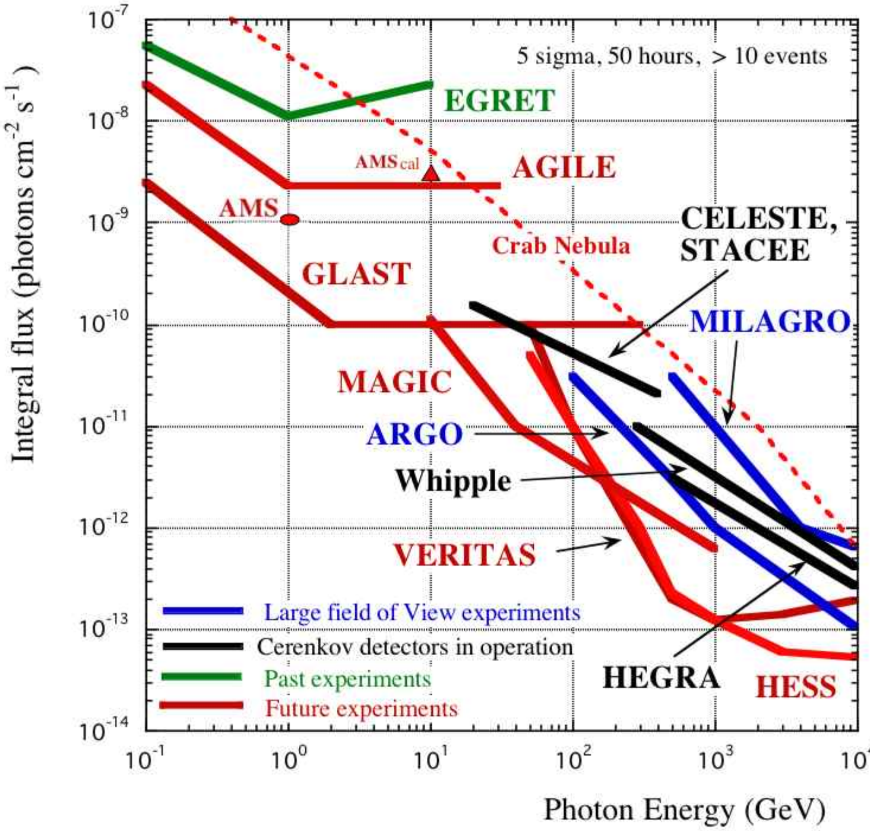


Figure 19: Sensitivity of present and future detectors in gamma-ray astrophysics (from Ref. [369]).

- CANGAROO-III is an array of four 10 m Cerenkov telescopes being constructed in Woomera, Australia [484]. It should start taking data in 2004.
- HESS consists of four 12 m diameter Cerenkov telescopes, at a site in the Gamsberg area of Namibia [485]. The telescopes are operational and started taking data.
- VERITAS is an array of 7 telescopes in construction on Kitt Peak in Arizona, USA [486]. A preliminary version, VERITAS-4, with 4 telescopes should be operative around 2006.

### 4.2.2 Space-based telescopes

The first gamma-ray space telescopes was EGRET (the Energetic Gamma-Ray Experiment Telescope), onboard the Compton gamma-ray observatory.

Launched in 1991, EGRET has observed the universe in a range of energies extending up to approximately 30 GeV, amassing a large catalog of observed gamma-ray sources, although around 60% of these sources remain unidentified.

The next space-based gamma-ray observatory will be GLAST (Gamma-ray Large Area Space Telescope), which is scheduled for launch in 2007. As for its predecessor, GLAST will detect gamma-rays by recording the characteristics of $e^+e^-$ pairs produced in the interaction of the incident gamma-ray with a dense layer of tungsten. GLAST's effective area to gamma-rays will be a full square meter, considerably larger than with EGRET. GLAST will have an angular resolution on the order of arcminutes, compared to the degree level with EGRET (energy resolution varies with energy for both experiments). Unlike EGRET, GLAST will be sensitive to gamma-rays up to several hundred GeV in energy.

GLAST is expected to be complementary to ground-based telescopes due to the lower range of energies observed, larger field of view, and higher duty cycle. We show in Fig.19 the sensitivity of some of the present and next generation ground-based and space-based gamma-ray experiments. We will use such information when discussing the prospects for indirect detection of particle dark matter.

## 4.3 Neutrino Telescopes

In addition to gamma-rays, neutrinos can be produced in the annihilations of dark matter particles. In this section, we review the status of high-energy neutrino telescopes, in particular, large volume Cerenkov detectors such as AMANDA, ANTARES and IceCube.

Neutrinos are considerably more difficult to observe than gamma-rays due to their weak interactions with ordinary matter. Neutrinos are not easily absorbed, however, allowing for their observation in underground, low background, experiments. In the GeV-TeV energy range, neutrinos are most easily observed by their "muon tracks" produced in charged current interactions inside of or nearby the detector volume. These muons travel through the detector emitting Cerenkov light which allows their trajectory to be reconstructed.

For a cosmic neutrino flux, $d\Phi_\nu/dE_\nu$, the rate of muon tracks in a detector is given by

$$\mathrm{rate} = \int_{\mathrm{E}_\mu^{\mathrm{thr}}} \mathrm{dE}_\nu \int_0^{1-\frac{\mathrm{E}_\mu^{\mathrm{thr}}}{\mathrm{E}_\nu}} \mathrm{dy}\, \mathrm{A}(\mathrm{E}_\mu) \mathrm{P}_\mu(\mathrm{E}_\nu, \mathrm{y}; \mathrm{E}_\mu^{\mathrm{thr}}) \frac{\mathrm{d}\Phi_\nu}{\mathrm{dE}_\nu}, \tag{90}$$

where $E_\mu^{\mathrm{thr}}$ is the muon threshold energy of the experiment (generally between 10 and 100 GeV), $A(E_\mu)$ is the effective area of the detector, typically in the range of 0.01 to 1.0 square kilometers (for further details and numerical values, see *e.g.* Ref. [51]) and $P_\mu(E_\nu, y;\, E_\mu^{\mathrm{thr}})$ is the probability that a neutrino of energy $E_\nu$ interacts with a nucleon producing a muon of energy $E_\mu \equiv (1-y)E_\nu$ above the detector threshold energy. As one would expect, this probability depends on the muon range, $R(E_\mu,\, E_\mu^{\mathrm{thr}})$, *i.e.* the distance travelled by muons before their energy drops below $E_\mu^{\rm thr}$. The function $P_\mu(E_\nu, y;\, E_\mu^{\rm thr})$ is thus given by

$$P_\mu(E_\nu, y;\, E_\mu^{\rm min}) = N_A\, R(E_\mu,\, E_\mu^{\rm min})\, \frac{d\sigma_{CC}^{\nu N}(E_\nu, y)}{dy} \tag{91}$$

where $N_A = 6.022 \times 10^{23}\, g^{-1}$ is Avogadro's number and $d\sigma_{CC}^{\nu N}(E_\nu, y)/dy$ is the differential cross section for neutrino–nucleon charged–current scattering.

The cross–section used in Eq. 91 is described in high-energy physics text-books, but carries uncertainties due to our limited knowledge of parton densities. It can be expressed as

$$\sigma^{\overset{(-)}{\nu} N}(s) = \int_0^1 dx \int_0^1 dy\, \frac{d^2\sigma^{\overset{(-)}{\nu} N}}{dx dy} \tag{92}$$

with

$$\frac{d^2\sigma^{\overset{(-)}{\nu} N}}{dx dy} = \frac{G_F^2 s}{2\pi}\, (1 + xys/M_W^2)^{-2} \big[(1-y) F_2^{\overset{(-)}{\nu}} + y^2 x F_1^{\overset{(-)}{\nu}} \pm y(1-\frac{y}{2}) x F_3^{\overset{(-)}{\nu}}\big] \tag{93}$$

where $F_i = F_i(x, Q^2 = xys)$ are the structure functions, $s = 2 M_N E_{\overset{(-)}{\nu}}$ and $G_F = 1.1663 \times 10^{-5}\,{\rm GeV}^{-2}$. For details regarding the calculation of high-energy neutrino-nucleon interactions including structure functions, see Ref. [235]).

The muon range, $R(E_\mu,\, E_\mu^{\rm min})$, appearing in Eq. 91 follows from the energy–loss equation [268]

$$-\, dE_\mu/dX = \alpha_\mu(E_\mu) + \beta_\mu(E_\mu)\, E_\mu, \tag{94}$$

with $X$ being the thickness of matter traversed by the muon, and the quantities $\alpha_\mu(E_\mu)$ and $\beta_\mu(E_\mu)$ are the ionization loss and the fractional energy loss coefficients, respectively. Integrating this result, we get the muon range

$$R(E_\mu,\, E_\mu^{\rm min}) \equiv X(E_\mu^{\rm min}) - X(E_\mu) = \frac{1}{\beta_\mu}\, \ln\, \frac{\alpha_\mu + \beta_\mu E_\mu}{\alpha_\mu + \beta_\mu E_\mu^{\rm min}}\,. \tag{95}$$

We adopt here the following values for the coefficients: $\alpha_\mu = 2.0 \times 10^{-3}$ GeV (cm we)$^{-1}$ (cmwe $\equiv g/{\rm cm}^2$) and $\beta_\mu = 6.0 \times 10^{-6}$ (cm we)$^{-1}$ [241].

We pass now to a brief description of existing and future neutrino telescopes, focusing on kilometer–scale experiments. The key idea is to detect muons, originating from neutrino fluxes as discussed above, building large arrays of photo–multipliers deep in the ice, in a lake or in the sea, to search for the Cerenkov light they are expected to emit as they move through these media.

The early pioneering effort made by the DUMAND collaboration [261] was followed by the deployment of the Lake Baikal experiment [52] and of AMANDA [30, 31] at the South Pole. Although these experiments have observed neutrinos

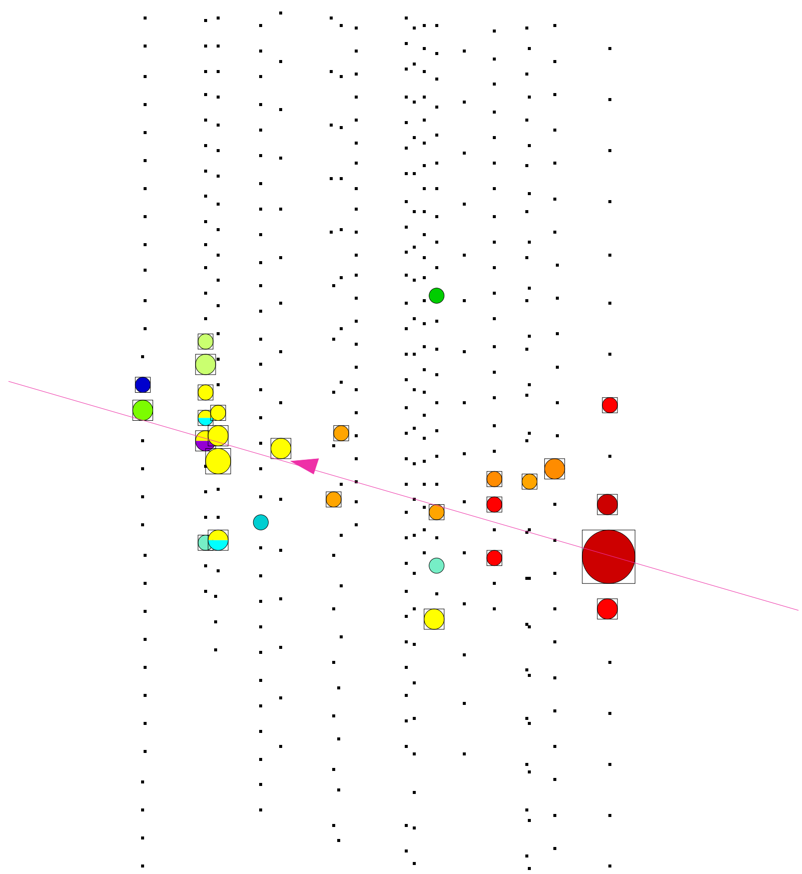

Figure 20: A muon neutrino event in AMANDA. Shown is the central part of the detector. The colorscale and symbol size correspond to hit time and amplitude [471].

produced in the Earth's atmosphere, they have not, thus far, identified any extra–terrestrial neutrinos.

AMANDA, with approximately 50,000 square meters of effective area (at trigger level) and a 30 GeV muon energy threshold, has been taking data for several years in its current configuration. ANTARES [41, 107], currently under construction in the Mediterranean, will have a similar effective area and a lower energy threshold of about 10 GeV. Unlike with experiments at the South Pole, ANTARES will be sensitive in the direction of the galactic center.

IceCube[17, 18], beginning construction in 2005, and scheduled for completion in 2010, will be the first kilometer scale high-energy neutrino telescope. Using technology similar to AMANDA, IceCube will be considerably more sensitive to dark matter annihilations than current experiments. Even larger, and perhaps lower threshold, experiments may be needed beyond IceCube to further search for evidence of dark matter annihilations. For a review of high-energy neutrino astronomy, see Refs. [271, 338].

## 4.4 Positron and Anti-Proton Experiments

Evidence for dark matter annihilations may also be observed in the spectra of cosmic positrons or anti-protons. Unlike gamma-rays and neutrinos, however, these charged particles do not point to their source due to the presence of galactic magnetic fields. Here we describe some of the experiments most important to these measurements.

The HEAT (High-Energy Antimatter Telescope) experiment made its first balloon flight in 1994-1995, measuring the spectrum of positrons between 1 and 30 GeV [60]. The results of this flight were very interesting, as they indicated an excess in the positron flux peaking at about 9 GeV and extending to higher energies. This excess could be a signature of dark matter annihilation in the local galactic halo (see section 6.5). A second HEAT flight in 2000 confirmed this observation [155, 156].

The BESS (Balloon borne Experiment Superconducting Solenoidal spectrometer) experiment has had several successful balloon flights since 1993, providing the most detailed measurements of the cosmic anti-proton spectrum to date in the range of about 200 MeV to 3 GeV [388, 353]. Above this energy, up to about 40 GeV, the CAPRICE experiment provides the best anti-proton measurements [116]. There appears to be a mild excess in the anti-proton spectrum in the hundreds of MeV range, although it is very difficult to assess this result with any certainty.

In the future, the experimental sensitivity to the cosmic positron and anti-proton spectra is likely to improve a great deal. Perhaps as early as 2005, the satellite borne PAMELA experiment, will begin its mission, measuring the spectra of both cosmic positrons and anti-protons with considerably improved precision. The primary objective of PAMELA is to the measure the cosmic anti-proton spectrum in the range of 80 MeV to 190 GeV and the cosmic positron spectrum in the range of 50 MeV to 270 GeV, far beyond the energies measured by HEAT, BESS or CAPRICE. In Fig. 21, we show the projected sensitivity of

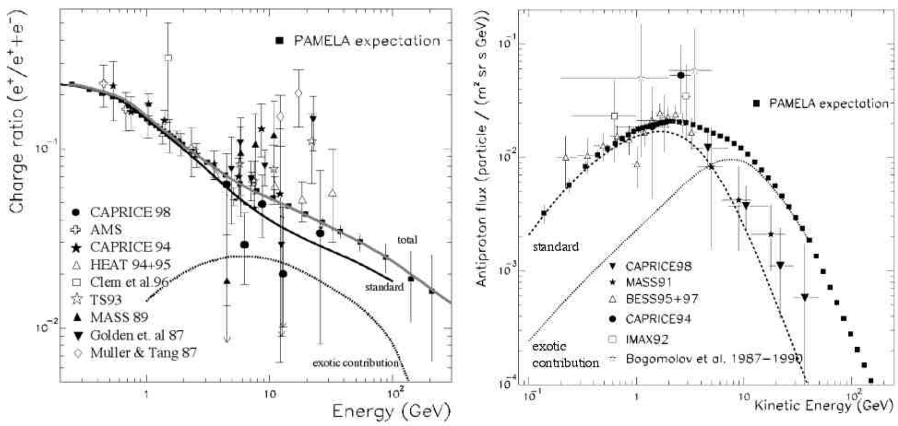


Figure 21: The projected ability of the PAMELA experiment to measure the spectra of cosmic positrons (left) and anti-protons (right). A contribution from annihilating neutralino dark matter is included in the spectra shown. Notice, in comparison to the measurements made by HEAT, CAPRICE, BESS and other experiments, the dramatic improvement in precision. Also note the reach to higher energies made possible with PAMELA. From Ref. [395].

PAMELA to cosmic positrons (left) and anti-protons (right). The results are shown assuming a contribution from annihilating neutralino dark matter. It is clear that PAMELA will measure these spectra to far greater precision than previous experiments, especially at high energies (above ~10 GeV).

AMS (the Alpha Magnetic Spectrometer) will considerably refine the measurement of the positron spectrum in its next manifestation, called AMS-02, onboard the International Space Station [62]. AMS-02, with a 5000 cm$^2$ sr aperture and a 1000 day duration, will provide exceptional precision in measuring the spectrum of cosmic positrons.

## 4.5 Observations at Radio Wavelengths

Observations at radio wavelengths belong to the realm of "classical" astronomy. Radio emission from the galactic halo, particularly from the galactic center, can provide a valuable probe of particle dark matter.

Electrons and protons produced in dark matter annihilations in the Galactic Centerregion will emit synchotron radiation (at radio wavelengths) as they propagate through the galactic magnetic fields (see section 6.2).

Rather than reviewing the subject of radio observations of the galactic halo, we refer to Cane (Ref. [131]) and to Brown (Ref. [125]), which also includes an interesting discussion of the absorption of radio emission at different wavelengths. A complete catalog of observations of the Galactic Center at all frequencies,

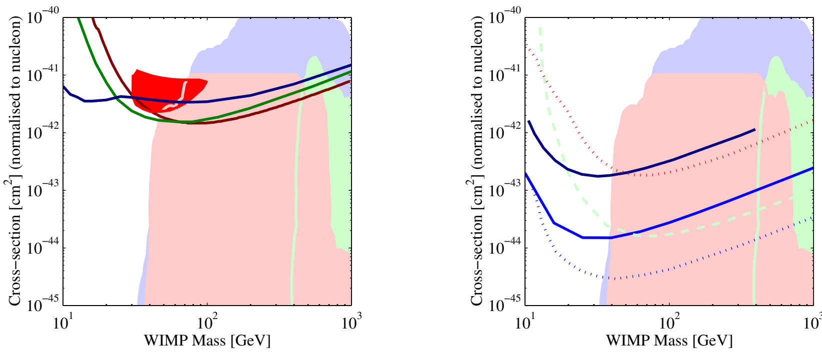


Figure 22: Current (left) and future (right) sensitivities of direct detection experiments. In the left frame, from top to bottom along the right side of the figure, the current limits from the CDMS, ZEPLIN-I and Edelweiss experiments are shown. The filled region near 30-100 GeV and $10^{-41}$ cm$^2$ is the parameter space favored by the DAMA experiment. In the right frame, from top to bottom along the right side of the figure, the projected reach of the GENIUS test facility (solid), CRESST-II (dots), CDMS-Soudan (solid), Edelweiss-II (dashed) and ZEPLIN-MAX (dots) are shown. In each frame, as filled regions, the space of models predicted by supersymmetry are shown [246]. The narrow region along the right side of the figure represents higgsino-like models, the region that reaches to the top of the figure represents mixed higgsino-gaugino models and the largest region represents gaugino-like models. These figures were made using the interface found at http://dendera.berkeley.edu/plotter/entryform.html.

and in particular at radio wavelengths, can be found in Ref. [375]. Additional information on specific measurements can be found in Refs. [167, 29, 337].

# 5 Direct Detection

Many direct detection experiments have already produced quite strong limits on the elastic scattering cross section with protons or neutrons of potential dark matter candidates. Furthermore, experiments in the coming years will improve on current limits by several orders of magnitude making the prospects for discovery very great.

Presently, the best direct detection limits come from the CDMS, Edelweiss and ZEPLIN-I experiments, shown in the left frame of Fig. 22. These limits are for spin-independent (scalar) interactions. With modern experiments, which use very heavy target nuclei, spin-dependent scattering experiments are not as sensitive to most dark matter candidates.

Also shown in the left frame of Fig. 22 is the region in which the DAMA experiment claims a discovery (see *e.g.* Ref. [83] for a recent review). DAMA, located at the INFN laboratories under the Gran Sasso mountain in Italy and